nature genetics

Direct measurement of transcription factor dissociation excludes a simple operator occupancy model for gene regulation

Petter Hammar[1,2], Mats Walldén[1,2], David Fange[1], Fredrik Persson[1], Özden Baltekin[1], Gustaf Ullman[1], Prune Leroy[1] & Johan Elf[1]

Transcription factors mediate gene regulation by site-specific binding to chromosomal operators. It is commonly assumed that the level of repression is determined solely by the equilibrium binding of a repressor to its operator. However, this assumption has not been possible to test in living cells. Here we have developed a single-molecule chase assay to measure how long an individual transcription factor molecule remains bound at a specific chromosomal operator site. We find that the *lac* repressor dimer stays bound on average 5 min at the native *lac* operator in *Escherichia coli* and that a stronger operator results in a slower dissociation rate but a similar association rate. Our findings do not support the simple equilibrium model. The discrepancy with this model can, for example, be accounted for by considering that transcription initiation drives the system out of equilibrium. Such effects need to be considered when predicting gene activity from transcription factor binding strengths.

Transcription factors are the major regulators of gene expression. Transcription factor–based regulation of transcription initiation is often described by a simple operator occupancy model, where in the case of repressors it is assumed that transcription is 'off' when the repressor is bound and 'on' when the promoter is free[1,2]. In this scenario, the resulting ratio of expression levels with and without repressor, i.e., the repression ratio (RR), becomes

$$\mathrm{RR} = \frac{\tau_{\mathrm{on}} + \tau_{\mathrm{off}}}{\tau_{\mathrm{on}}} \qquad (1)$$

where τ_{off} is the average time the repressor is bound and τ_{on} is the average time the promoter is free (**Supplementary Note**). The repression ratio is high when the repressor is bound for a long time (large τ_{off}) or when the repressor concentration is high, which leads to fast binding (small τ_{on}). This simple equation has a central position in quantitative biology as it relates the state of the cell, i.e., transcription factor concentrations, to change in state, i.e., gene expression. The equation is therefore used in most synthetic and systems biology studies although the underlying assumptions have not been tested in living cells, where cooperative binding, active transcription, DNA replication and chromosome dynamics could influence gene regulation.

The challenge of testing the operator occupancy model in living cells is to measure the rates of operator association, τ_{on}^{-1}, and dissociation, τ_{off}^{-1}, directly in live cells rather than inferring them from reporter expression assays[3,4]. Recently, we developed a direct single-molecule microscopy assay to measure the rate of binding to a single *lac* operator site in the bacterial chromosome[5]. Here we present an *in vivo* version of a biochemical chase assay[6], which enables direct measurements of spontaneous dissociation of the *lac* repressor protein, LacI, from individual chromosomal operator sites (**Fig. 1a**,**b**). In our assay, operator-bound fluorescent LacI-YFP dimers that spontaneously dissociate are replaced (chased) by non-fluorescent LacI tetramers. Non-fluorescent LacI molecules are present in excess (**Supplementary Fig. 1a**) and prevent rebinding of fluorescent LacI. The spontaneous dissociation process can thus be followed by counting the average number of bound fluorescent molecules per cell over time. To start the experiment with the fluorescent LacI bound, a point mutation has been introduced into the fluorescent LacI such that it cannot bind the inducer isopropyl β-D-1-thiogalactopyranoside (IPTG)[7]. The presence of IPTG prevents binding of the non-fluorescent LacI until IPTG is removed at the start of the experiment (**Supplementary Fig. 1b**,**c**). To ensure that dissociation kinetics were independent of IPTG outflux, we showed that the intracellular concentration of IPTG within 1 min of its removal dropped to a level where non-fluorescent LacI bound effectively (**Supplementary Fig. 2** and **Supplementary Note**), and we subsequently analyzed dissociation kinetics beginning at 1.5 min after the removal of IPTG. An extended analysis of how the finite concentrations of non-fluorescent LacI influenced the results is provided in the Online Methods. The model for replication-induced LacI dissociation is extended in the **Supplementary Note**. The kinetic assays were performed on *E. coli* cells residing in a microfluidic growth chamber (**Fig. 1c**,**d**), which allowed the cells to

[1]Department of Cell and Molecular Biology, Science for Life Laboratory, Uppsala University, Uppsala, Sweden. [2]These authors contributed equally to this work. Correspondence should be addressed to J.E. (johan.elf@icm.uu.se).

Received 21 July 2013; accepted 31 January 2014; published online 23 February 2014; doi:10.1038/ng.2905

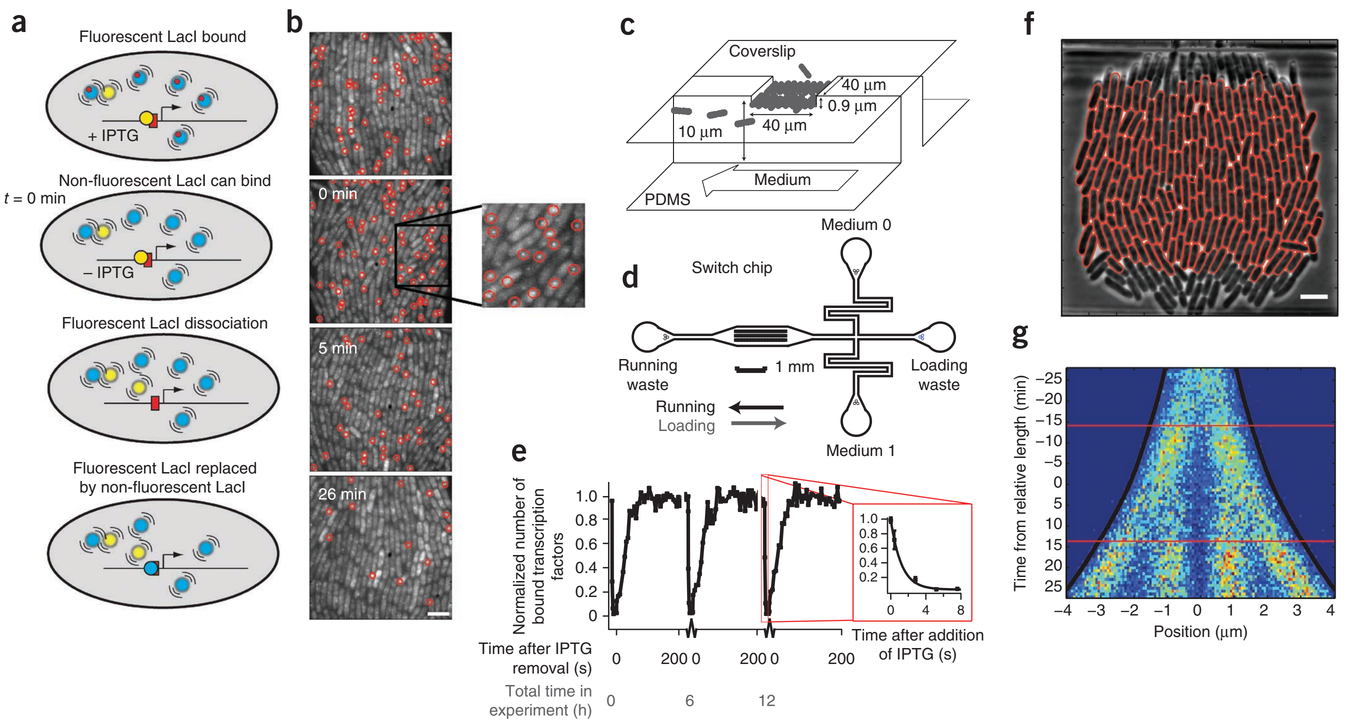

Figure 1 The single-molecule chase assay. (**a**) Outline of the single-molecule chase assay. When fluorescent LacI dimers (yellow) dissociate from the *lac* operator (red box), they are replaced by non-fluorescent wild-type LacI tetramers (blue) present in excess. (**b**) Examples of fluorescence images (4-s exposure) taken before and at different time points after the removal of IPTG. Scale bar, 4 μm. The inset image is magnified by 2× relative to the original image. Red circles indicate detected operator-bound LacI-YFP. (**c**,**d**) The microfluidic switching chip (**d**) contains 51 traps as illustrated (**c**). Each trap harbors ~250 *E. coli* cells and allows for sustained exponential growth and fast change of medium. (**e**) Medium switch–induced transcription factor dissociation and association. When medium is switched from high 2-nitrophenyl β-D-fucopyranoside (ONPF; anti-inducer) to high IPTG (inducer), transcription factors dissociate in a few seconds (inset). When medium is switched back, transcription factors associate in ~30 s. The graph shows three switching cycles separated by 6-h recovery periods. (**f**) Automatically segmented cells using a phase-contrast image. Scale bar, 4 μm. (**g**) Intracellular positions of bound LacI-YFP molecules (*x* axis) mapped to the cell replication cycle (*y* axis). Individual cell replication cycles are synchronized so that the time of 0 min always implies a cell length of 4.25 μm. Horizontal lines mark the average times for cell divisions.

be maintained in a constant state of exponential growth (generation time of 26 min)[8] as well as allowing rapid medium exchange (in 2 s). Image acquisition and medium exchange were automated and synchronized so that the experiment was repeatable with high precision (**Fig. 1e**). Cell segmentation and detection of fluorescent spots were also automated and enabled the mapping of individual molecules onto an intracellular coordinate system for an arbitrary number of cells (**Fig. 1f**). For example, **Figure 1g** (as well as **Supplementary Fig. 3**) shows the probability distribution of the intracellular location of specifically bound LacI-YFP molecules as a function of position in the cell cycle.

We used the *in vivo* chase assay to measure the kinetics for two operators of different strength, the natural $lacO_1$ operator and the stronger, symmetric artificial $lacO_{sym}$ operator. The dissociation curves for the LacI-YFP dimer from the $lacO_1$ and $lacO_{sym}$ operators at 37 °C are shown in **Figure 2a**. The average time LacI stayed bound to its operator (τ_{off}) was 5.3 ± 0.2 (s.e.m.) min for $lacO_1$ and 9.3 ± 0.4 (s.e.m.) min for $lacO_{sym}$. The average time before the operator was bound by a repressor (τ_{on}) was measured under identical experimental conditions (**Fig. 2b**) and was 30.9 ± 0.5 (s.e.m.) s for $lacO_1$ and 27.6 ± 0.6 (s.e.m.) s for $lacO_{sym}$. Thus, a stronger operator has a slower dissociation rate but a similar association rate.

We were then ready to ask whether the measured association and dissociation times could be used to predict the repression ratio using the simple operator occupancy model, i.e., equation (1), as given by the model in **Figure 3a** without any cooperative interaction between LacI and RNA polymerase (RNAP) ($\omega = 1$, as defined in **Fig. 3a** and equations (3) and (4) in the Online Methods). Combining the association and dissociation measurements, we calculated that the repression ratio was expected to be 11.2 ± 0.5 (s.e.m.) for $lacO_1$ and 21.2 ± 0.9

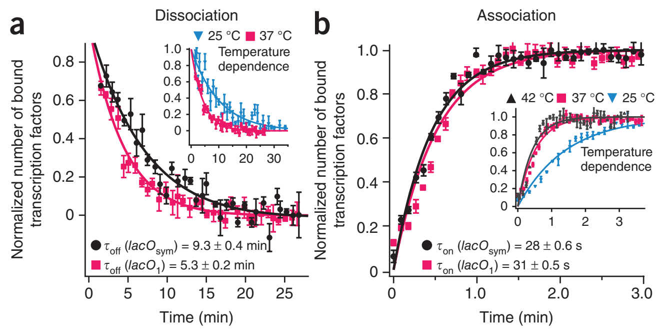

Figure 2 Kinetic measurements for individual *lac* operators. (**a**) Dissociation curves for $lacO_{sym}$ and $lacO_1$. $n = \{i, j, k\}$ implies i repetitions 6 h apart for chip 1, j repetitions for chip 2 and k repetitions for chip 3. Error bars, ± s.e.m.; $n = \{2, 3, 2\}$ ($lacO_1$) and $n = \{3, 2, 3\}$ ($lacO_{sym}$). Inset, temperature dependence for dissociation from $lacO_1$. Error bars, ± s.e.m.; $n = \{2, 3, 2\}$ (37 °C) and $n = \{2, 2\}$ (25 °C). (**b**) Association curves for $lacO_{sym}$ and $lacO_1$. Error bars, ± s.e.m.; $n = \{2, 3, 2\}$ ($lacO_1$) and $n = \{3, 2, 3\}$ ($lacO_{sym}$). Inset, temperature dependence for association with $lacO_1$. Error bars, ± s.e.m.; $n = \{2, 3, 2\}$ (37 °C) and $n = \{3\}$ (25 and 42 °C).

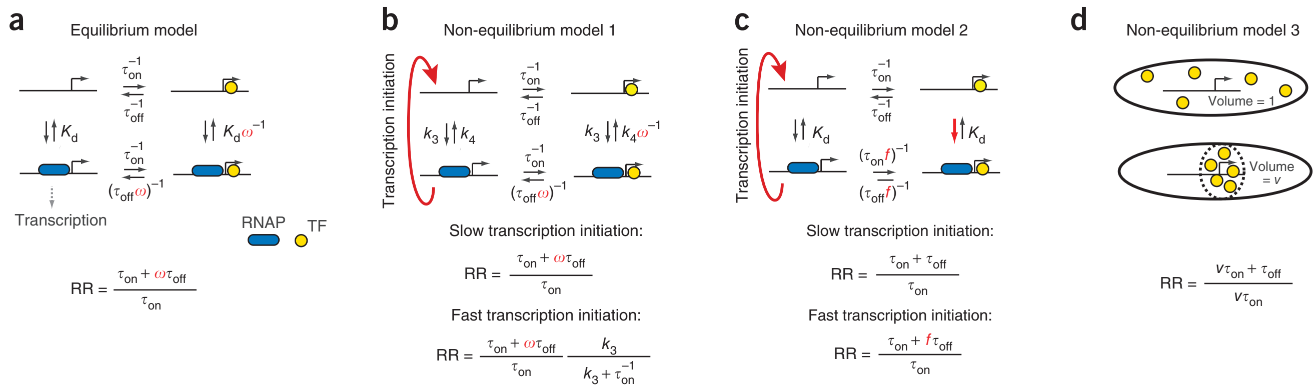

Figure 3 Models of gene regulation. (**a**) At equilibrium, the repression ratio only depends on the fraction of time the operator is bound independent of kinetic schemes. Owing to cooperative binding ($\omega > 1$), the ratio can be modulated by other factors. TF, transcription factor; K_d, equilibrium binding constant. (**b**) Transcription initiation can drive the system out of equilibrium such that the repression ratio depends on the rate of transcription initiation. (**c**) The transcription factor binds and dissociates slower when RNAP is bound. Transcription drives the system out of equilibrium such that the transcription factor associates at naked DNA and dissociates at RNAP-bound DNA. (**d**) When the transcription factors are maintained in a reduced volume, v, transcription factor association rates are in the simplest case increased by the corresponding factor.

(s.e.m.) for $lacO_{sym}$ (**Table 1**). The corresponding measurements of the repression ratios for the LacI-Venus dimer based on an enzymatic reporter assay were 10.0 ± 1.3 (s.e.m.) for $lacO_1$ and 29.7 ± 3.4 (s.e.m.) for $lacO_{sym}$ (**Table 1**). We conclude that the operator occupancy model accounts for the repression ratio for $lacO_1$ but not for the ratio for $lacO_{sym}$, where the observed repression ratio was higher than expected when considering association and dissociation rates alone.

This discrepancy for $lacO_{sym}$ motivated the construction of more complex interaction models. One possibility was an equilibrium model where LacI interacts cooperatively with RNAP or another protein binding near the operator and where the degree of cooperativity depends on the operator sequence. This model is represented (**Fig. 3a**) using $\omega = 1.5$ and $\omega = 1$ for $lacO_{sym}$ and $lacO_1$, respectively, and resulted in excellent agreement with the measured repression ratios. Such a difference in cooperativity between $lacO_1$ and $lacO_{sym}$ could be due to the markedly different bending of DNA when LacI is bound to the different operators[8,9]. Operator sequence–specific interactions between LacI and RNAP have previously been suggested when the operator is positioned upstream of the p*lac*UV5 promoter[10]. Although this equilibrium mechanism is also possible with the operator located downstream of the promoter, a model with operator-specific cooperativity was not needed to describe our data. Cellular reaction dynamics are commonly out of equilibrium, and we therefore also considered more simple non-equilibrium schemes. In **Figure 3b–d**, we outline three such schemes that can increase the repression ratio beyond the ratio predicted by the simple operator occupancy model. We discuss them individually below.

The first non-equilibrium scheme (**Fig. 3b**) is similar to the scheme with cooperative interaction with RNAP (**Fig. 3a**) except that active transcription initiation clears the promoter in the absence of LacI. Slow transcription initiation leads to a repression ratio as in the cooperative equilibrium model, whereas fast transcription initiation leads to a reduced repression ratio, as it is possible to synthesize transcripts before the repressor has equilibrated with DNA. Interestingly, we found that the transcription rate for the *lac* operon with full induction was 5.4 ± 0.5 (s.e.m.) times higher in the strain with the $lacO_1$ sequence than in the strain with the $lacO_{sym}$ sequence next to the promoter (**Supplementary Note**). This difference in transcription rate, in combination with the measured association and dissociation rates, is sufficient to fully account for the measured repression ratios when $\omega = 1.5$ for both $lacO_1$ and $lacO_{sym}$. The reason for this is that $lacO_{sym}$ is closer to the equilibrium case (with slow transcription) described above, whereas $lacO_1$ is out of equilibrium (with fast transcription) and thus has a lower repression ratio than what is expected from the equilibrium model alone (**Fig. 3b**). As a consequence, no operator sequence–dependent interaction between LacI and RNAP is needed in this case, as the sequences are transcribed at different rates.

Also in the second non-equilibrium scheme (**Fig. 3c**), transcription initiation drives the system out of equilibrium but this time without any cooperative binding between RNAP and LacI. In this scheme, RNAP binds to one of the alternative *lac* promoters next to the operator-bound LacI but does not continue into open complex formation[11]. In contrast, when RNAP binds in the absence of LacI, it proceeds rapidly and irreversibly into transcription, clearing the promoter. Consequently, LacI will most often bind in an RNAP-free promoter region and dissociate from an RNAP-bound operator region. Thus,

Table 1 Comparison of repression ratios from reporter expression assays and direct single-molecule *in vivo* measurements

	Repression ratio		Single-molecule kinetics	
Operator region	Reporter expression assay[a]	$\frac{\tau_{on}+\tau_{off}}{\tau_{on}}$	τ_{on} (s)	τ_{off} (min)
$lacO_1$	10.0 ± 1.3	11.2 ± 0.5	30.9 ± 0.5	5.3 ± 0.2
$lacO_{sym}$	29.7 ± 3.4	21.2 ± 0.9	27.6 ± 0.6	9.3 ± 0.4

Data are shown as mean values ± s.e.m.; n indicates replicates from individual experiments (reporter expression): $n = 9$ ($lacO_1$) and $n = 8$ ($lacO_{sym}$). See **Figure 2** for details of the single-molecule experiments.
[a]The repression ratio is induced (+ IPTG) divided by repressed (– IPTG) *lacZ* expression in terms of Miller units (normalized β-galactosidase activity) and is normalized to the lower repressor concentrations in the kinetic experiments (**Supplementary Fig. 8** and **Supplementary Note**).

Table 2 Binding kinetics dependence on roadblocks

	τ_{on} (s)	τ_{off} (min)	Repression ratio
Without roadblock	27.6 ± 0.6	9.3 ± 0.4	21.2 ± 0.9
With roadblock	37.1 ± 0.6	11.6 ± 1.4	19.7 ± 1.1

Association and dissociation rates measured for LacI-YFP with or without TetR binding next to one side of the operator $lacO_{sym}$. Data are shown as mean values ± s.e.m.; $n = \{i, j, k\}$ implies i repetitions 6 h apart for chip 1, j repetitions for chip 2 and k repetitions for chip 3: $n = \{4, 2\}$ (τ_{on}, $lacO_{sym}$ with roadblock) and $n = \{4, 3, 3\}$ (τ_{off}, $lacO_{sym}$ with roadblock). Data without roadblock are the same as in **Table 1**.

if a bound RNAP molecule slows down LacI dissociation, this would result in repression beyond that predicted in the equilibrium model, even if the binding strength for LacI is unaltered by the bound RNAP. The average times for LacI association and dissociation are expected to increase by up to a factor of two when a protein is bound next to the *lac* operator, as sliding along DNA in and out of the operator is blocked from one side[5]. To test this hypothesis, we positioned the *tet* repressor protein, TetR, next to the *lac* operator site and measured the times for LacI dissociation and association. We found that the time for association increased by a factor $f = 1.35 \pm 0.04$ (s.e.m.) when TetR was bound next to $lacO_{sym}$ and that the effect on dissociation was similar (**Table 2** and **Supplementary Fig. 4**), as was expected from detailed balance when steady-state binding is not altered. The effect was smaller ($f = 1.16 \pm 0.03$ (s.e.m.)) for $lacO_1$, for which the lower binding probability reduced the impact of the diffusion blockade, as the transcription factor will need multiple attempts to bind anyway[5]. If RNAP binds in a closed complex near LacI and blocks sliding in the same way as TetR, repression ratios would be expected to increase up to 12.8 ± 0.6 (s.e.m.) and 28.2 ± 1.4 (s.e.m.) for $lacO_1$ and $lacO_{sym}$, respectively, from this effect alone.

In the third scheme (**Fig. 3d**), active transport or a combination of slow diffusion and degradation maintains a higher concentration of LacI close to the operator sites. This higher concentration of LacI can lead to faster association rates than we report above, as our association process started from any position in the cells when IPTG dissociated from LacI. A local gradient effect is expected to be greater for $lacO_{sym}$ than for $lacO_1$ as LacI is more likely to bind $lacO_{sym}$ before escaping to a random position[5]. Furthermore, previous studies have reported that the spatial distribution of LacI in the cell under poor growth conditions depends on where in the chromosome the protein is encoded[12,13]. However, under our experimental conditions, we could not observe any difference in the spatial distributions of non-operator-bound LacI expressed from different chromosomal loci with different intracellular locations (**Supplementary Fig. 5** and **Supplementary Note**). Using single-particle tracking, we also did not observe that LacI could be trapped locally in the nucleoid for more than a few seconds. This timeframe is far shorter than what would be required to maintain a locally higher concentration of LacI close to the point of synthesis (**Supplementary Fig. 6**). In addition, we did not observe a change in the repression of the LacI-regulated *lacZYA* operon when the *lacI* gene was moved to its mirror position on the other chromosome arm (**Supplementary Note**). Together, these results make it unlikely that LacI association is faster under steady-state growth than in our measurements owing to local concentration gradients of the repressor.

Our single-molecule chase method has allowed us to identify inconsistencies in the simple operator occupancy model of gene regulation in living *E. coli* cells, a model system where it is possible to conduct the experiment with sufficient accuracy. The inconsistencies are most easily explained by simple non-equilibrium mechanisms driven by transcription initiation itself. The same mechanisms are expected to operate in eukaryotic cells, where the added complexities of ATP-dependent chromatin remodeling[14] and clearing of the transcription factor binding region by divergent transcription[15] will contribute to keeping operator occupancy out of equilibrium. Overall, non-equilibrium transcription factor kinetics add a new layer of complexity to the genomics puzzle beyond the steady-state mapping of transcription factor concentrations to gene activity.

METHODS

Methods and any associated references are available in the online version of the paper.

Note: Any Supplementary Information and Source Data files are available in the online version of the paper.

ACKNOWLEDGMENTS
We thank K.S. Matthews for advice on LacI mutants, G.-W. Li for helpful comments, X.S. Xie (Harvard University) for the MalI-Venus strain and I. Barkefors for critical reading of the manuscript. This work was supported by the European Research Council (ERC), the Knut and Alice Wallenberg Foundation (KAW), Vetenskapsrådet (VR), the Foundation for Strategic Research (SSF) and the Göran Gustafsson Foundation.

AUTHOR CONTRIBUTIONS
J.E. conceived the project, J.E. and P.H. conceived the chase method, M.W. designed the microfluidics chip, P.H. and P.L. generated strains, P.H., M.W., Ö.B., F.P. and P.L. performed experiments, F.P., G.U., D.F. and M.W. developed and implemented analysis routines, P.H., F.P., M.W., G.U., D.F. and Ö.B. analyzed the data, J.E. and D.F. developed theoretical models, and J.E., P.H., D.F., M.W. and F.P. wrote the manuscript.

COMPETING FINANCIAL INTERESTS
The authors declare no competing financial interests.

1. Bintu, L. *et al.* Transcriptional regulation by the numbers: applications. *Curr. Opin. Genet. Dev.* **15**, 125–135 (2005).
2. Oehler, S., Amouyal, M., Kolkhof, P., von Wilcken-Bergmann, B. & Muller-Hill, B. Quality and position of the three *lac* operators of *E. coli* define efficiency of repression. *EMBO J.* **13**, 3348–3355 (1994).
3. Oehler, S., Eismann, E.R., Kramer, H. & Muller-Hill, B. The three operators of the *lac* operon cooperate in repression. *EMBO J.* **9**, 973–979 (1990).
4. Choi, P.J., Cai, L., Frieda, K. & Xie, X.S. A stochastic single-molecule event triggers phenotype switching of a bacterial cell. *Science* **322**, 442–446 (2008).
5. Hammar, P. *et al.* The Lac repressor displays facilitated diffusion in living cells. *Science* **336**, 1595–1598 (2012).
6. Riggs, A.D., Bourgeois, S. & Cohn, M. The *lac* repressor-operator interaction. 3. Kinetic studies. *J. Mol. Biol.* **53**, 401–417 (1970).
7. Chang, W.I., Barrera, P. & Matthews, K.S. Identification and characterization of aspartate residues that play key roles in the allosteric regulation of a transcription factor: aspartate 274 is essential for inducer binding in *lac* repressor. *Biochemistry* **33**, 3607–3616 (1994).
8. Bell, C.E. & Lewis, M. A closer view of the conformation of the Lac repressor bound to operator. *Nat. Struct. Biol.* **7**, 209–214 (2000).
9. Bell, C.E. & Lewis, M. Crystallographic analysis of Lac repressor bound to natural operator *O1*. *J. Mol. Biol.* **312**, 921–926 (2001).
10. Garcia, H.G. *et al.* Operator sequence alters gene expression independently of transcription factor occupancy in bacteria. *Cell Reports* **2**, 150–161 (2012).
11. Sanchez, A., Osborne, M.L., Friedman, L.J., Kondev, J. & Gelles, J. Mechanism of transcriptional repression at a bacterial promoter by analysis of single molecules. *EMBO J.* **30**, 3940–3946 (2011).
12. Kuhlman, T.E. & Cox, E.C. Gene location and DNA density determine transcription factor distributions in *Escherichia coli*. *Mol. Syst. Biol.* **8**, 610 (2012).
13. Hermsen, R., ten Wolde, P.R. & Teichmann, S. Chance and necessity in chromosomal gene distributions. *Trends Genet.* **24**, 216–219 (2008).
14. Vignali, M., Hassan, A.H., Neely, K.E. & Workman, J.L. ATP-dependent chromatin-remodeling complexes. *Mol. Cell. Biol.* **20**, 1899–1910 (2000).
15. Seila, A.C., Core, L.J., Lis, J.T. & Sharp, P.A. Divergent transcription: a new feature of active promoters. *Cell Cycle* **8**, 2557–2564 (2009).

ONLINE METHODS

Strain construction. Strains were constructed in a BW25993 background[16] using the λ Red[16] or pKO3 (ref. 17) protocols. Detailed strain descriptions can be found in the **Supplementary Note**, **Supplementary Figure 7** and **Supplementary Table 1**.

Growth conditions. Cells were grown in M9 minimal liquid medium supplemented with 0.4% glucose and RPMI amino acids (Sigma). For growth of strains harboring pBAD24 plasmids encoding *lacI*, *lacI-Venus* or *xylR*, the medium was supplemented with carbenicillin (Sigma).

For microfluidics experiments, saturated (overnight) cultures were diluted 1:200 in 40 ml of medium and grown at 37 °C for 4 h unless otherwise specified. Cells were collected by centrifugation and immediately loaded onto microfluidic chips as previously described[18].

Information about growth conditions in other microscopy experiments and expression assays can be found in the **Supplementary Note**.

Fluorescence microscopy and microfluidics. *Microfluidic switching chips—design and preparation*. Microfabrication of the templates and construction of the individual devices were performed in accordance with the protocols described previously[18] with the exception that an extra medium port was added to allow for rapid exchange of medium. Inert polystyrene beads of 2 μm in diameter (Sigma-Aldrich) were added to one medium reservoir. Beads allowed for the detection of flow rates and flow directions necessary for determining the induction states of the device during operation.

Relative height differences between medium reservoirs were used to control the pressure gradients and, thereby, flow rates and directions in the device during running and medium exchange. Medium exchange, i.e., anticorrelated elevation/lowering of reservoirs, was automated by using programmable linear actuators (Robocylinder, Intelligent Actuators), the control of which was synchronized with image acquisition using a custom-written Java program.

Optical setup. We used a Nikon Eclipse T*i*-E microscope (with Nikon's Apo TIRF 100×/1.49 oil immersion objective) equipped with a dichroic mirror (Chroma t515.5rdc), an excitation filter (Chroma 514/10), an emission filter (Chroma 550/50) and an EMCCD camera (iXon EM+ DU-897 from Andor). The camera was cooled to −80 °C, and the linearized electron-multiplying gain was set to 150. A 2× magnification lens was placed in the emission path before the camera. Fluorescence was excited by a Coherent Innova-304 Ar^+-laser at 514 nm. When measuring association and dissociation rates, the power was 15 W/cm^2 using 4-s exposures. For single-particle tracking, the power was 650 W/cm^2, and, for overnight growth experiments, the power was <5 W/cm^2 (see the **Supplementary Note** for details). A second camera (Scion Corp) was used for external phase-contrast imaging. The microscope was enclosed in an OkiLab cage incubator where the set temperature was maintained at 37 ± 0.1 °C, 42 ± 0.1 °C or 25.5 ± 0.3 °C. Image acquisition was controlled by the open-source software μManager[19] in combination with custom-written acquisition scripts.

Spot detection. We used á Trous wavelet three-plane decomposition[20] and detected the spots in the second wavelet plane. Significant wavelet coefficients were determined through scale-dependent $k\sigma$ thresholding where σ is the s.d. of the second wavelet plane, estimated by the MAD estimate[21], and $k = 3$ (association experiments) or $k = 4$ (dissociation experiments).

LacI-Venus kinetics using automated switching of medium. Experiments were started when cells had grown to fill the whole microfluidic traps. For a fast and well-defined switch of medium, the medium reservoirs were connected to linear actuators and controlled from the computer in parallel with μManager-run imaging acquisition.

For the analysis of operator-bound single LacI molecules in fusion with the fluorescent protein, YFP-derived Venus[22] (LacI-Venus), spots were detected as described above. Because the traps of the microfluidic chip were full with densely packed cells, we normalized the number of spots per trap by total cell area.

Association with a single operator. The principle of the experiment was essentially as presented previously[5,23] with the exception that the experiment was performed in the microfluidic device to allow for direct comparison with the corresponding dissociation experiment at 37 °C. The experiment was started by switching the medium for the induced cells from one containing IPTG to one containing the competitor ONPF at a 1 mM concentration. The addition of ONPF at high concentration was used to ensure that the association rate was not limited by the time it took for IPTG to leave the cell. Cells were imaged with 4-s exposures with a frame rate of ~0.18 frames/s. Fluorescent spots were counted as described above, and binding curves with data from the same strain were fitted (Igor Pro (v6.12A)) to the single exponential function $y = a(1-be^{-kt})$, where a and b were independent for each series and k was the same for all series. Experiments were repeated to generate sufficient statistical power to test the hypothesis. For visualization in **Figure 2b**, the a and b parameters were used to normalize the data points in individual series before calculating the average and s.e.m. for each time point and plotting together with the fitted curve.

In **Supplementary Figure 2c**, the rate of LacI-Venus association is plotted as a function of the added ONPF concentration, and the plot shows that a 1 mM concentration is saturating. It also shows that LacI binds 1 min faster with the addition of ONPF at a saturating concentration, which suggests that it takes up to 1 min for the intracellular IPTG concentration to drop to a level where LacI can bind the operator. This timing is important for the dissociation assay described below. The relative difference in LacI-Venus concentration between strains is described in the **Supplementary Note** and **Supplementary Figure 8**.

Chase assay for the measurement of dissociation rates. In the *in vivo* chase experiment, LacI-Venus molecules are first bound to individual, single operator sites; then, through competition with non-fluorescent wild-type LacI in excess, they can be seen to dissociate as the number of fluorescent spots decreases. The chase experiment relies on the possibility of inducing binding of non-fluorescent LacI in a well-defined timeframe while LacI-Venus is already bound. To accomplish this, a single point substitution was introduced in the *lac* repressor gene (encoding LacI p.Asp274Asn), which causes more than a 1,000-fold reduction in IPTG affinity without changing operator binding strength[7]. The gene (referred to as *lacI*$_s$) was expressed in fusion with Venus, resulting in a chromosomally expressed LacI$_s$-Venus that does not dissociate, even in the presence of 1 mM IPTG (**Supplementary Fig. 1c**). Wild-type LacI was expressed from an arabinose-inducible promoter on the plasmid pBAD24.

The ratio between LacI$_s$-Venus and wild-type LacI monomers when the plasmid was uninduced is seen at time 0 in **Supplementary Figure 1a**. When the plasmid was fully induced for a long time, the competitor copy number became so high that either 1 mM IPTG did not saturate LacI to prevent operator binding or the LacI$_s$-Venus–LacI heterodimers, which naturally form (and are dominant when LacI is overexpressed) and bind one IPTG molecule, did not bind the operator. When instead XylR was expressed from pBAD24, LacI$_s$-Venus was unaffected by IPTG (**Supplementary Fig. 1c**).

Before the switch, with IPTG present, LacI$_s$-Venus homodimer bound the operator. When IPTG was removed at $t = 0$, there was a short (1-min) period of increased binding (**Supplementary Fig. 1b**). This increased binding is probably due to the association of heterodimers (in competition with non-fluorescent wild-type LacI) to available operator sites. Because of this initial association and the time delay required to reduce the intracellular IPTG concentration to a level where non-fluorescent LacI bound (see below and **Supplementary Fig. 2**), we fit the dissociation process from 1.5 min after switching to medium without IPTG to an exponential decay process that also took into account the fact that the transcription factor was displaced once per generation owing to replication. The implications of the approximation are quantified below and in the **Supplementary Note**. Experiments were repeated to generate sufficient statistics to test the hypothesis.

Time-dependent excess of non-fluorescent LacI. We induced the expression of non-fluorescent LacI at time 0 (medium containing 1 mM IPTG was switched to medium containing 0.2% arabinose). This switch resulted in a time-dependent increase in the concentration of the non-fluorescent LacI chase molecules (**Supplementary Fig. 1a**). This time-dependent increase motivated us to calculate how this would influence the measured dissociation kinetics.

The equations that describe the probabilities that an operator is initially bound by a fluorescent molecule (P_F), that it is empty (P_E) or that it is occupied by a non-fluorescent molecule (P_N) were

$$\begin{aligned}
\frac{dP_F(t)}{dt} &= \tau_{on}^{-1}P_E - \tau_{off}^{-1}P_F \\
\frac{dP_E(t)}{dt} &= \tau_{off}^{-1}(P_F + P_N) - \tau_{on}^{-1}(1 + q(t))P_E \\
\frac{dP_N(t)}{dt} &= q(t)\tau_{on}^{-1}P_E - \tau_{off}^{-1}P_N \\
\frac{dP_F(0)}{dt} &= 1, \frac{dP_E(0)}{dt} = 0, \frac{dP_N(0)}{dt} = 0
\end{aligned} \quad (2)$$

Here $q(t)$ is the fold excess of non-fluorescent transcription factor, which was measured directly by protein blot (**Supplementary Fig. 1a**) and is closely approximated by $q(t) = 4 + t^2$, where t is the time in minutes after the addition of IPTG.

For an infinitely high q, P_F will decay as a pure exponential with rate τ_{off}^{-1} starting from $t = 0$. For a finite q, the observed dissociation process is slightly slower. When fitting a single exponential function to the solution of $P_F(t)$, using parameters from **Table 1**, starting from 1.5 min and ending at 20 min, the dissociation rate is underestimated by up to 11% for *lacO*$_1$ and by up to 9% for *lacO*$_{sym}$ owing to the finite concentration of non-fluorescent LacI. This underestimation would change the predicted repression ratios (based on the simple operator occupancy model) to 10.2 for *lacO*$_1$ and 19.4 for *lacO*$_{sym}$, which do not alter the conclusions drawn when assuming large excess of non-fluorescent LacI.

Models. *Cooperative LacI binding*. Consider the scheme in **Figure 3a**,**b** written in further detail.

$$\begin{array}{ccc}
\mathrm{O} & \underset{k_2 = \tau_{off}^{-1}}{\overset{k_1 = \tau_{on}^{-1}}{\rightleftarrows}} & \mathrm{O \cdot TF} \\
k_3\downarrow\uparrow k_4 & & k_3\downarrow\uparrow \omega^{-1}k_4 \\
\mathrm{O \cdot RNAP} & \underset{\omega^{-1}k_2 = \omega^{-1}\tau_{off}^{-1}}{\overset{k_1 = \tau_{on}^{-1}}{\rightleftarrows}} & \mathrm{O \cdot TF \cdot RNAP} \\
k_6\downarrow & &
\end{array} \quad (3)$$

Here LacI and RNAP bind ω times longer when they are binding at the same time. The repression ratio in this non-equilibrium scheme is

$$\mathrm{RR} = 1 + \frac{k_1(k_1 + k_2 + k_3 + k_4 + k_6)(k_3 + k_4\omega^{-1})}{k_2\omega^{-1}(k_1 + k_2 + k_3 + k_4)(k_3 + k_4 + k_6)} \quad (4)$$

If we assume that transcription initiation is slow where $k_6 \to 0$ (equilibrium case),

$$\mathrm{RR} = 1 + \frac{\omega k_1(k_3 + k_4\omega^{-1})}{k_2(k_3 + k_4)} \xrightarrow{k_3 \gg k_4} 1 + \frac{\omega k_1}{k_2} = 1 + \frac{\omega\tau_{off}}{\tau_{on}} \quad (5)$$

If we assume that transcription initiation is fast where $k_6 \to \infty$ (far from equilibrium case),

$$\begin{aligned}
\mathrm{RR} &= 1 + \frac{k_1(\omega k_3 + k_4)}{k_2(k_1 + k_2 + k_3 + k_4)} \xrightarrow{k_3 \gg k_4} 1 + \frac{\omega k_1}{k_2}\frac{k_3}{k_1 + k_2 + k_3} \\
&\approx 1 + \frac{\omega k_1}{k_2}\frac{k_3}{k_1 + k_3}
\end{aligned} \quad (6)$$

These are the limiting approximations given in the main text (**Fig. 3a**,**b**). To see what we obtained with specific numbers, we used the measured τ_{on} and τ_{off} values and assumed that $\omega = 1.5$, $k_3 = 1\ \mathrm{min}^{-1}$ and $k_4 = 0.1\ \mathrm{min}^{-1}$. These numbers gave RR = 10.0 and an induced transcription initiation rate of 0.61 min^{-1} (refs. 24,25) when $k_6 = 1.7\ \mathrm{min}^{-1}$ for *lacO*$_1$ and RR = 28.2 and an induced transcription initiation rate of 0.61/5.4 min^{-1} for *lacO*$_{sym}$ when $k_6 = 0.14\ \mathrm{min}^{-1}$. The value of 5.4 is the measured difference in expression between the induced *lac* operon controlled by *lacO*$_1$ and *lacO*$_{sym}$.

Non-equilibrium model with roadblock. Consider the scheme in **Figure 3c** written in further detail.

$$\begin{array}{ccc}
\mathrm{O} & \underset{k_2 = \tau_{off}^{-1}}{\overset{k_1 = \tau_{on}^{-1}}{\rightleftarrows}} & \mathrm{O \cdot TF} \\
k_3\downarrow\uparrow k_4 & & k_3\downarrow\uparrow k_4 \\
\mathrm{O \cdot RNAP} & \underset{f^{-1}k_2 = f^{-1}\tau_{off}^{-1}}{\overset{f^{-1}k_1 = f^{-1}\tau_{on}^{-1}}{\rightleftarrows}} & \mathrm{O \cdot TF \cdot RNAP} \\
k_6\downarrow & &
\end{array} \quad (7)$$

The repression ratio RR is

$$\mathrm{RR} = \frac{\frac{k_1(k_3 + k_4)(k_4 + k_6)}{k_2(k_3 + k_4 + k_6)} + k_4 + f^{-1}(k_1 + k_2 + k_3)\left(\frac{k_1(k_3 + k_4)}{k_2(k_3 + k_4 + k_6)} + 1\right)}{f^{-1}(k_1 + k_2 + k_3) + k_4} \quad (8)$$

Assuming that the system is far from equilibrium, such that $k_6 \gg k_3 + k_4$, and that the transcription initiation rate is fast enough, such that $k_1(k_3 + k_4)/(k_2k_6) \ll 1$, then the repression ratio is

$$\mathrm{RR} = 1 + \frac{k_1(k_3 + k_4)}{k_2(k_4 + f^{-1}(k_2 + k_3 + k_1))} \quad (9)$$

Further, assuming that RNAP binding is strong, such that $k_3 \gg k_4$, that the turnover of RNAP is faster than the turnover of the transcription factor, such that $k_3 \gg k_1 + k_2$, and that f is not very much smaller than 1, then the repression ratio is

$$\mathrm{RR} = 1 + \frac{fk_1}{k_2} = 1 + \frac{f\tau_{off}}{\tau_{on}} \quad (10)$$

16. Datsenko, K.A. & Wanner, B.L. One-step inactivation of chromosomal genes in *Escherichia coli* K-12 using PCR products. *Proc. Natl. Acad. Sci. USA* **97**, 6640–6645 (2000).
17. Link, A.J., Phillips, D. & Church, G.M. Methods for generating precise deletions and insertions in the genome of wild-type *Escherichia coli*: application to open reading frame characterization. *J. Bacteriol.* **179**, 6228–6237 (1997).
18. Ullman, G. *et al.* High-throughput gene expression analysis at the level of single proteins using a microfluidic turbidostat and automated cell tracking. *Phil. Trans. R. Soc. Lond. B* **368**, 20120025 (2013).
19. Edelstein, A., Amodaj, N., Hoover, K., Vale, R. & Stuurman, N. Computer control of microscopes using microManager. *Curr. Protoc. Mol. Biol.* **Chapter 14**, Unit14.20 (2010).
20. Olivo-Marin, J.C. Extraction of spots in biological images using multiscale products. *Pattern Recognit.* **35**, 1989–1996 (2002).
21. Sadler, B.M. & Swami, A. Analysis of multiscale products for step detection and estimation. *IEEE Trans. Inf. Theory* **45**, 1043–1051 (1999).
22. Nagai, T. *et al.* A variant of yellow fluorescent protein with fast and efficient maturation for cell-biological applications. *Nat. Biotechnol.* **20**, 87–90 (2002).
23. Elf, J., Li, G.W. & Xie, X.S. Probing transcription factor dynamics at the single-molecule level in a living cell. *Science* **316**, 1191–1194 (2007).
24. Taniguchi, Y. *et al.* Quantifying *E. coli* proteome and transcriptome with single-molecule sensitivity in single cells. *Science* **329**, 533–538 (2010).
25. Yu, J., Xiao, J., Ren, X., Lao, K. & Xie, X.S. Probing gene expression in live cells, one protein molecule at a time. *Science* **311**, 1600–1603 (2006).